Supporting information

Supramolecular construction of cyanide-bridged Re^{I} diimine multichromophores

Kristina S. Kisel,[†,‡] Alexei S. Melnikov,[§] Elena V. Grachova,[†] Antti J. Karttunen,[,ǁ] Antonio Doménech-Carbó,[⊥] Kirill Yu. Monakhov,[≠] Valentin G. Semenov,[†] Sergey P. Tunik,[†] Igor O. Koshevoy[*,‡]*

[†] Institute of Chemistry, St. Petersburg State University, Universitetskiy pr. 26, Petergof, St. Petersburg, Russia

[‡] Department of Chemistry, University of Eastern Finland, 80101 Joensuu, Finland

[§] Peter the Great St. Petersburg Polytechnic University, Polytechnicheskaya, 29, St. Petersburg, Russia

[ǁ] Department of Chemistry and Materials Science, Aalto University, 00076 Aalto, Finland

[⊥] Universidad de Valencia, Dr. Moliner 50, 46100, Burjassot, Valencia, Spain

[≠] Leibniz Institute of Surface Engineering (IOM), Permoserstraße 15, 04318 Leipzig, Germany

E-mail: antti.karttunen@aalto.fi; igor.koshevoy@uef.fi

Figure S11. Electron density difference plots for $S_0 \rightarrow S_1$ and $T_1 \rightarrow S_0$ transitions of complexes **5** and **6**.

Figure S12. $S_0 \rightarrow S_1$ electron density difference plots of complexes **7–9**.

Table S5. HOMO–LUMO gaps and computational photophysical results for complexes **1–9**.

Figure S13. Normalized emission (top) and excitation (bottom) spectra of complexes **1** and **2** in dichloromethane at 298K.

Figure S14. Excitation and emission spectra of complexes **1–3** and **5–8** (CH_2Cl_2, 77K).

Figure S15. Excitation and emission spectra of complex **4** in the solid state (298K).

Figure S16. A: cyclic voltammograms of solutions of complexes **9** and **10**. B: the voltammetric response of the $Fe^{II/III}$ couple. C: cyclic voltammograms of microparticulate films of **9** and **10**.

Figure S17. Temperature dependence of $\chi_m T$ of complex **10**.

Table S1. Crystal data and structure refinement for **2−10**.

Identification code	**2**	**3**	**4**	**5**	**6**
CCDC	1873814	1873819	1873820	1873812	1873816
Empirical formula	$C_{32}H_{16}F_3N_5O_9Re_2S$	$C_{135}H_{98}F_6N_{10}O_{15}P_4Re_4S_2$	$C_{35}H_{23}AuF_3N_3O_6PReS$	$C_{59}H_{34}Au_2Cl_2F_6N_{12}O_{18}Re_4S_2$	$C_{33}H_{16}AuF_3N_6O_9Re_2S$
Formula weight	1075.96	3147.03	1084.76	2586.73	1298.94
Temperature (K)	150(2)				
Wavelength (Å)	0.71073				
Crystal system	Monoclinic	Monoclinic	Triclinic	Triclinic	Triclinic
Space group	$P2_1/n$	$P2_1/n$	$P\bar{1}$	$P\bar{1}$	$P\bar{1}$
Unit cell dimensions					
a (Å)	11.5861(3)	18.4637(3)	13.7488(11)	6.7123(2)	9.6102(4)
b (Å)	29.9030(9)	17.9475(3)	17.1139(13)	14.4404(4)	11.1701(5)
c (Å)	12.2138(4)	21.5171(3)	18.6538(15)	19.2307(5)	21.0631(9)
a (°)	90.000(0)	90.000(0)	104.436(4)	83.8120(10)	82.053(2)
β (°)	114.3330(10)	99.5750(10)	107.647(4)	81.2440(10)	82.562(2)
γ (°)	90.000(0)	90.000(0)	107.157(4)	77.3120(10)	87.010(2)
Volume ($Å^3$)	3855.7(2)	7030.94(19)	3709.7(5)	1791.94(9)	2219.15(17)
Z	4	2	4	1	2
ρ_{calc} (Mg/m^3)	1.854	1.487	1.942	2.397	1.944
μ (mm^{-1})	6.396	3.576	7.372	11.030	8.849
F(000)	2032	3088	2056	1194	1200
Crystal size (mm^3)	0.426 × 0.408 × 0.232	0.428 × 0.225× 0.183	0.795 × 0.222× 0.194	0.736 × 0.476× 0.294	0.784 × 0.131 × 0.119

θ range for data collection (°)	2.281 to 30.000	1.347 to 27.999	1.234 to 30.000	2.684 to 35.000	0.984 to 25.049
Index ranges	-16<=h<=16, -42<=k<=42, -17<=l<=15	-24<=h<=24, -23<=h<=23, -28<=l<=28	-19<=h<=19, -24<=k<=24, -26<=l<=26	-10<=h<=10, -23<=k<=23, -30<=l<=31	-11<=h<=11, -13<=k<=13, -25<=l<=25
Reflections collected	41009	158783	161209	54252	61619
Independent reflections	11176 [R(int) = 0.0282]	16972 [R(int) = 0.0657]	21621 [R(int) = 0.0505]	15704 [R(int) = 0.0249]	7838 [R(int) = 0.0521]
Completeness to θ = 25.24°	99.0 %	99.9%	100.0 %	99.8 %	99.8 %
Absorption correction	Numerical				
Max. and min. transmission	0.318 and 0.171	0.561 and 0.310	0.329 and 0.067	0.140 and 0.45	0.419 and 0.055
Refinement method	Full-matrix least-squares on F^2				
Data/ restrains/ parameters	11176 / 61 / 542	17804 / 0 / 775	21621 / 43 / 907	15704 / 0 / 487	7838 / 0 / 496
GOOF on F^2	1.097	1.031	1.022	1.073	1.084
Final R indices [I>2σ(I)][a]	R1 = 0.0307, wR2 = 0.0641	R1 = 0.0278, wR2 = 0.0699	R1 = 0.0307, wR2 = 0.0725	R1 = 0.0190, wR2 = 0.0400	R1 = 0.0454, wR2 = 0.1023
R indices (all data)	R1 = 0.0362, wR2 = 0.0660	R1 = 0.0420, wR2 = 0.0737	R1 = 0.0479, wR2 = 0.0804	R1 = 0.0230, wR2 = 0.0412	R1 = 0.0520, wR2 = 0.1050
Largest diff. peak and hole (e.Å^{-3})	2.143 and -2.285	1.755 and -0.750	2.226 and -1.989	1.040 and -1.798	2.305 and -3.640

[a] $R_1 = \Sigma||F_o| - |F_c||/\Sigma|F_o|$; $wR2 = [\Sigma\ [w(F_o^2 - Fc^2)^2]/\ \Sigma[w(F_o^2)^2]]^{1/2}$

Table S1. Continued.

Identification code	**7**	**8**	**9**	**10**
CCDC	1873815	1873818	1873817	1873813
Empirical formula	$C_{58}H_{32}F_6N_{12}O_{18}PtRe_4S_2$	$C_{70}H_{42}F_6N_{12}O_{19}PtRe_4S_2$	$C_{86}H_{48}F_6FeN_{18}O_{24}Re_6S_2$	$C_{87}H_{48}F_9FeN_{18}O_{27}Re_6S_3$
Formula weight	2302.96	2473.16	3068.59	3217.66
Temperature (K)	150(2)			
Wavelength (Å)	0.71073			
Crystal system	Triclinic	Monoclinic	Orthorhombic	Triclinic
Space group	$P\bar{1}$	$C2/m$	$Pccn$	$P\bar{1}$
Unit cell dimensions				
a (Å)	9.1122(10)	26.155(7)	15.3876(5)	15.1248(16)
b (Å)	13.7593(15)	23.777(7)	26.4331(11)	15.1433(16)
c (Å)	15.7554(17)	15.634(4)	26.8849(11)	16.093(3)
a (°)	73.691(4)	90.000(0)	90.000(0)	102.913(4)
β (°)	75.256(3)	92.781(6)	90.000(0)	104.068(4)
γ (°)	77.300(3)	90.000(0)	90.000(0)	117.313(3)
Volume ($Å^3$)	1809.9(3)	9711(5)	10935.2(7)	2927.0(7)
Z	1	4	4	1
ρ_{calc} (Mg/m^3)	2.113	1.692	1.864	1.825
μ (mm^{-1})	8.734	6.519	6.863	6.437
F(000)	1072	4648	5776	1517
Crystal size (mm^3)	0.367 × 0.281× 0.136	0.285 × 0.260× 0.214	0.321 × 0.140 × 0.129	0.869× 0.112 × 0.056

θ range for data collection (°)	2.341 to 29.999	1.158 to 29.000	1.515 to 26.000	2.104 to 25.999
Index ranges	-12<=h<=12, -19<=k<=19, -22<=l<=22	-35<=h<=35, -32<=k<=32, -21<=l<=21	-13<=h<=18, -32<=k<=20, -32<=l<=33	-18<=h<=18, -18<=h<=18, -19<=l<=19
Reflections collected	43057	102798	60847	40107
Independent reflections	10443 [R(int) = 0.0260]	13221 [R(int) = 0.0533]	10746 [R(int) = 0.0436]	11442 [R(int) = 0.0669]
Completeness to θ = 25.24°	99.6 %	100.0 %	99.9 %	99.5 %
Absorption correction	Numerical			
Max. and min. transmission	0.383 and 0.142	0.336 and 0.258	0.471 and 0.217	0.714 and 0.071
Refinement method	Full-matrix least-squares on F^2			
Data/ restrains/ parameters	10443 / 0 / 457	13221 / 0 / 532	10746 / 143 / 710	11442 / 28 / 718
GOOF on F^2	1.029	1.015	1.164	1.017
Final R indices [I>2σ(I)][a]	R1 = 0.0178, wR2 = 0.0414	R1 = 0.0266, wR2 = 0.0555	R1 = 0.0384, wR2 = 0.0746	R1 = 0.0460, wR2 = 0.1101
R indices (all data)	R1 = 0.0216, wR2 = 0.0428	R1 = 0.0414, wR2 = 0.0606	R1 = 0.0569, wR2 = 0.0849	R1 = 0.0852, wR2 = 0.1273
Largest diff. peak and hole (e.Å^{-3})	2.125 and -0.879	1.401 and -1.510	1.649 and -0.910	2.303 and -2.373

[a] $R_1 = \Sigma||F_o| - |F_c||/\Sigma|F_o|$; $wR2 = [\Sigma [w(F_o^2 - Fc^2)^2]/ \Sigma[w(F_o^2)^2]]^{1/2}$

Table S2. Selected bond lengths and angles for **2−6** (two values for **4** named A and B correspond to two independent molecules found in the unit cell). For simplicity, the model shown on the right was used to summarize structural data.

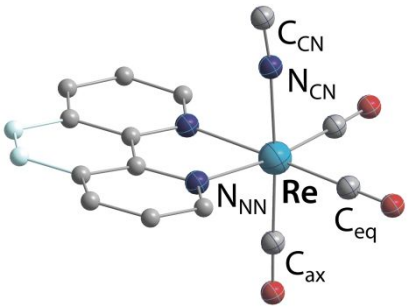

	2		3		4		5		6	
Bond lengths, Å										
	Re¹	Re²	Re¹	Re²	Re^A	Re^B	Re¹	Re²	Re¹	Re²
Re-N_{NN}	2.173(3)/2.184(3)	2.172(3)/2.177(4)	2.180(3)/2.187(3)	2.176(3)/2.192(3)	2.174(3)/2.175(4)	2.167(4)/2.178(4)	2.1636(16)/2.1675(16)	2.1623(16)/2.1732(17)	2.161(9)/2.197(8)	2.161(9)/2.181(9)
Re-N_{CN}	-	2.120(4)	-	2.108(3)	2.130(3)	2.125(4)	2.1257(17)	2.1249(17)	2.119(9)	2.132(10)
Re-C_{eq}	1.917(4)/1.923(4)	1.909(5)/1.920(5)	1.889(4)/1.896(4)	1.885(4)/1.886(3)	1.921(5)/1.936(5)	1.916(5)/1.934(6)	1.926(2)/1.928(2)	1.917(2)/1.927(2)	1.940(13)/1.955(12)	1.902(13)/1.917(12)
Re-C_{ax}	1.945(4)	1.935(4)	-	-	1.925(4)	1.933(5)	1.914(2)	1.919(2)	1.924(13)	1.923(13)
	M = Re				M = Au					
M-C_{CN}	2.110(3)	-	2.081(3)	-	2.004(4)	1.999(4)	1.973(2)	1.968(2)	1.963(11)	1.968(12)
M-P	-	-	2.3784(9)	2.3868(9)	2.2752(10)	2.2705(11)	-	-	-	-
Bond angles, °										
	Re¹	Re²	Re¹	Re²	Re^A	Re^B	Re¹	Re²	Re¹	Re²
N_{NN}-Re-N_{NN}	75.45(12)	75.63(14)	75.22(10)	75.68(10)	75.70(13)	75.96(14)	75.08(6)	75.21(6)	75.9(3)	75.7(3)
N_{NN}-Re-N(C)$_{CN}$	83.04(13)/84.23(13)	84.27(12)/85.31(14)	83.62(11)/83.69(11)	82.84(11)/83.85(11)	81.62(13)/81.70(13)	82.90(14)/84.81(14)	80.66(6)/84.16(6)	79.66(7)/83.54(6)	82.4(3)/83.0(3)	82.3(3)/83.0(3)
C_{eq}-Re-N(C)$_{CN}$	92.68(14)/93.96(15)	93.20(17)/93.97(15)	92.93(15)/95.04(14)	92.52(13)/93.81(13)	92.07(16)/94.34(17)	91.33(17)/94.11(18)	91.39(8)/96.90(6)	92.21(8)/95.52(8)	91.0(4)/93.0(4)	91.8(5)/92.5(5)
C_{ax}-Re-N(C)$_{CN}$	176.08(15)	176.85(16)	-	-	176.55(16)	177.64(17)	175.24(8)	175.83(8)	177.5(4)	176.5(5)
Re-N_{CN}-C_{CN}	176.0(3)		176.8(3)		178.0(4)	177.2(4)	167.81(17)	171.88(18)	176.9(9)	177.8(10)
P-Re-N(C)$_{CN}$	-	-	173.84(9)	174.85(8)	-	-	-	-	-	-
C_{CN}-Au-C_{CN}	-		-		-		175.27(9)		177.2(5)	

Table S3. Selected bond lengths and angles for **7−10**. For simplicity, the model shown on the right was used to summarize structural data.

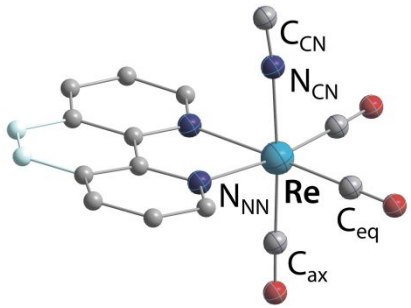

	7		8			9			10		
Bond lengths, Å											
	Re[1]	Re[2]	Re[1]	Re[2]	Re[3]	Re[1]	Re[2]	Re[3]	Re[1]	Re[2]	Re[3]
Re-N_{NN}	2.172(2)/2.177(2)	2.161(2)/2.175(2)	2.175(3)/2.175(3)	2.177(3)/2.189(3)	2.172(3)/2.172(3)	2.154(6)/2.171(6)	2.177(6)/2.183(6)	2.172(6)/2.174(6)	2.159(7)/2.175(7)	2.180(8)/2.187(9)	2.161(8)/2.177(7)
Re-N_{CN}	2.138(2)	2.141(2)	2.141(4)	2.132(3)	2.124(5)	2.121(6)	2.132(6)	2.114(6)	2.135(7)	2.128(7)	2.143(9)
Re-C_{eq}	1.918(3)/1.919(3)	1.923(3)/1.927(3)	1.922(4)/1.922(4)	1.921(4)/1.925(4)	1.932(5)/1.932(5)	1.916(9)/1.918(9)	1.923(9)/1.932(9)	1.916(8)/1.921(8)	1.910(10)/1.911(12)	1.906(10)/1.940(12)	1.908(12)/1.946(11)
Re-C_{ax}	1.919(3)	1.913(3)	1.915(5)	1.911(4)	1.919(6)	1.897(8)	1.920(8)	1.910(8)	1.918(10)	1.910(10)	1.898(11)
	M = Pt					M = Fe					
M-C_{CN}	1.988(3)	1.979(3)	1.985(5)	1.977(3)	1.983(5)	1.918(8)	1.937(7)	1.916(7)	1.923(8)	1.947(9)	1.918(9)
Bond angles, º											
	Re[1]	Re[2]	Re[1]	Re[2]	Re[3]	Re[1]	Re[2]	Re[3]	Re[1]	Re[2]	Re[3]
N_{NN}-Re-N_{NN}	75.03(8)	75.33(8)	75.41(14)	75.87(11)	75.40(18)	75.1(2)	74.6(2)	75.3(2)	75.2(3)	75.9(4)	75.0(3)
N_{NN}-Re-N_{CN}	85.59(8)/85.90(8)	83.62(8)/85.71(8)	79.06(11)/79.06(11)	81.53(10)/81.54(11)	83.46(14)/83.46(14)	84.3(2)/85.1(2)	84.1(2)/85.2(2)	84.1(2)/84.1(2)	83.7(3)/84.2(3)	83.3(3)/83.9(3)	83.7(3)/87.5(3)
C_{eq}-Re-N_{CN}	91.80(11)/94.15(9)	90.56(10)/91.59(10)	96.38(14)/96.38(14)	93.71(14)/94.99(13)	93.06(17)/93.06(17)	93.3(3)/95.0(3)	93.2(3)/95.3(3)	90.0(3)/95.8(3)	88.6(4)/93.6(3)	93.1(3)/95.8(3)	91.1(4)/94.2(4)
C_{ax}-Re-N_{CN}	177.95(11)	179.15(10)	173.99(18)	175.96(14)	177.6(3)	172.9(3)	175.6(3)	173.9(3)	176.2(3)	176.6(3)	176.6(4)
Re-N_{CN}-C_{CN}	174.3(2)	169.9(2)	159.7(4)	173.7(3)	176.3(5)	174.2(6)	177.1(6)	166.5(6)	168.2(7)	178.4(7)	172.5(7)
	M = Pt					M = Fe					
M-C_{CN}- N_{CN}	174.7(2)	173.2(2)	179.9(4)	176.8(3)	173.3(5)	176.7(6)	176.9(7)	176.1(6)	172.2(8)	177.0(8)	178.1(8)
C_{CN}-M-C_{CN}	86.36(10)		89.45(10)/90.71(10)			88.4(3)/89.0(3)/89.7(3)			87.3(3)/91.2(3)/91.3(3)		

Table S4. Comparison of calculated and XRD bond distances of complexes **2–9**. Only distances involving Re, Pt, Fe, or P atoms are listed. The numbering corresponds to the XYZ files given as Supporting Information.

Complex	Bond	Exp. (Å)	Calc. (Å)
2	Re(32) - N(2) ≡ C	2.12	2.13
	Re(32) - C(33) = O	1.94	1.98
	Re(32) - C(34/35) = O	1.91	1.94
	Re(32) - N(36/37)	2.17	2.21
	Re(3) - C(1) ≡ N	2.11	2.15
	Re(3) - C(4) = O	1.95	1.95
	Re(3) - C(5/6) = O	1.92	1.94
	Re(3) - N(7/8)	2.18	2.21
3	Re(3) - N(2) ≡ C	2.11	2.12
	Re(3) - C(4/5)	1.89	1.92
	Re(3) - N(6/7)	2.18	2.21
	Re(3) - P(57)	2.39	2.41
	P(57) - Ph(58/59)	1.83	1.86
	P(57) - Ph(60)	1.84	1.85
	Re(30) - C(1) ≡ N	2.08	2.08
	Re(30) - C(31/32)	1.89	1.92
	Re(30) - N(33/34)	2.18	2.21
	Re(30) - P(91)	2.38	2.47
	P(91) - Ph(92/93)	1.84	1.86
	P(91) - Ph(94)	1.84	1.84
4	Re(4) - N(3) ≡ C	2.13	2.14
	Re(4) - C(5) = O	1.93	1.94
	Re(4) - C(6/7) = O	1.93	1.94
	Re(4) - N(8/9)	2.17	2.21
	P(33) - Au(1)	2.27	2.34
	P(33) - Ph(34/35)	1.81	1.84
	P(33) - Ph(36)	1.81	1.82
	Au(1) - C(2) ≡ N	2.00	2.02
5	Au(1) - C(2/3)	1.97	2.00
	Re(6/33) - N(4/5) ≡ C	2.13	2.14
	Re(6/33) - C(7/34)	1.92	1.95
	Re(6/33) - C(8/9/35/36)	1.92	1.94
	Re(6/33) - N(10/11/37/38)	2.17	2.20
6	Au(1) - C(2/3)	1.97	2.00
	Re(6/33) - N(4/5) ≡ C	2.13	2.14
	Re(6/33) - C(7/34)	1.92	1.95
	Re(6/33) - C(8/9/35/36)	1.93	1.94
	Re(6/33) - N(10/11/37/38)	2.18	2.21
7	Pt - C	1.98	2.00
	Re - N ≡ C	2.14	2.14
	Re - C (side)	1.92	1.93
	Re - C (opp.)	1.92	1.95
	Re - N(x2)	2.17	2.20
8	Pt - C	1.98	2.00
	Re - N ≡ C	2.13	2.15
	Re - C (side)	1.91	1.95
	Re - C (opp.)	1.93	1.93
	Re - N(x2)	2.18	2.21
9	Fe - C	1.92	1.91
	Re - N ≡ C	2.13	2.14
	Re - C (side)	1.92	1.93
	Re - C (opp.)	1.91	1.95
	Re - N(x2)	2.17	2.21

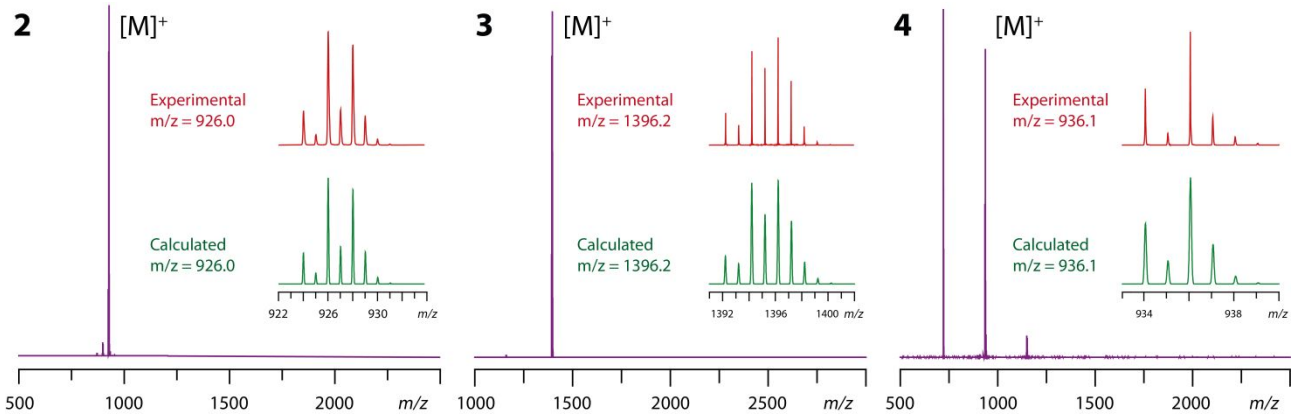

Figure S1. ESI–MS for complexes **2**−**4**.

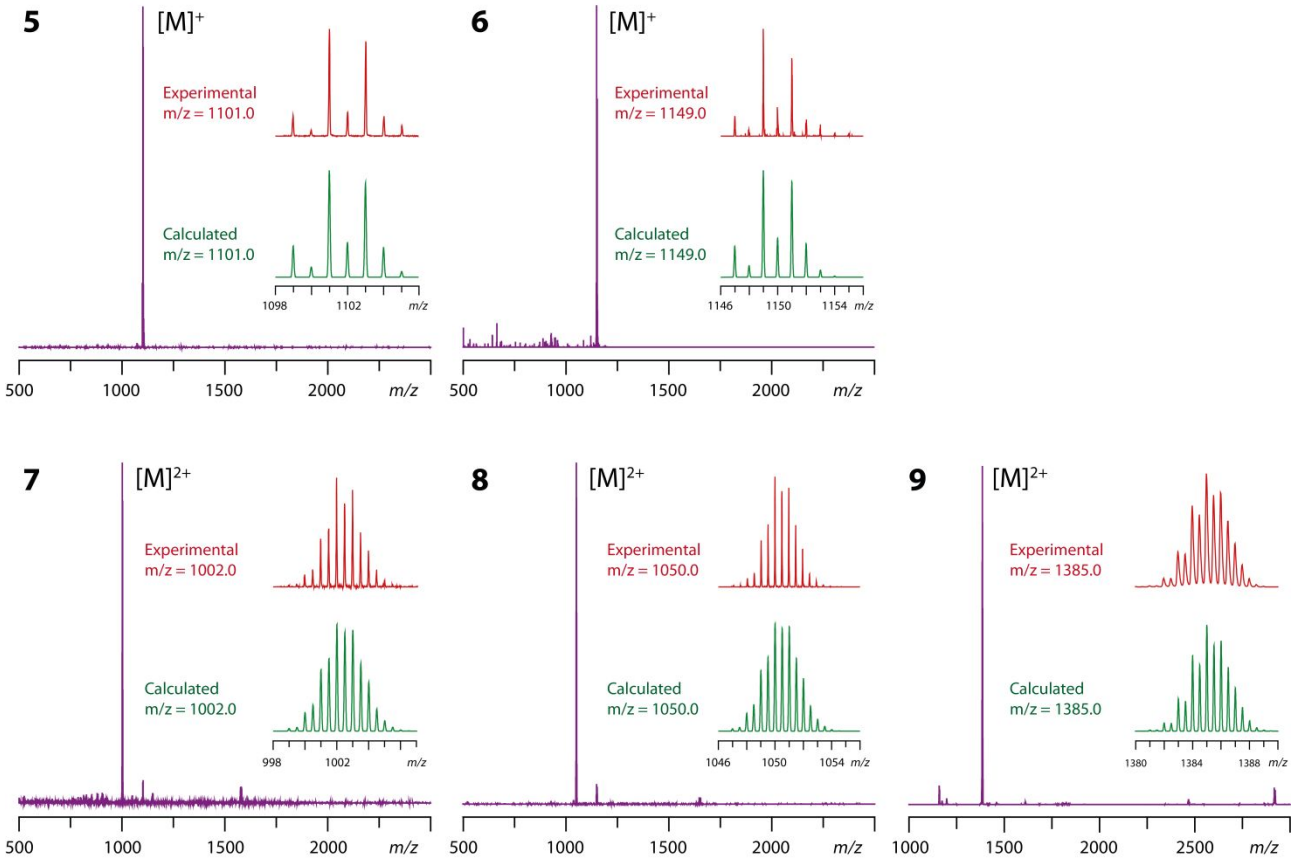

Figure S2. ESI–MS for complexes **5**−**9**.

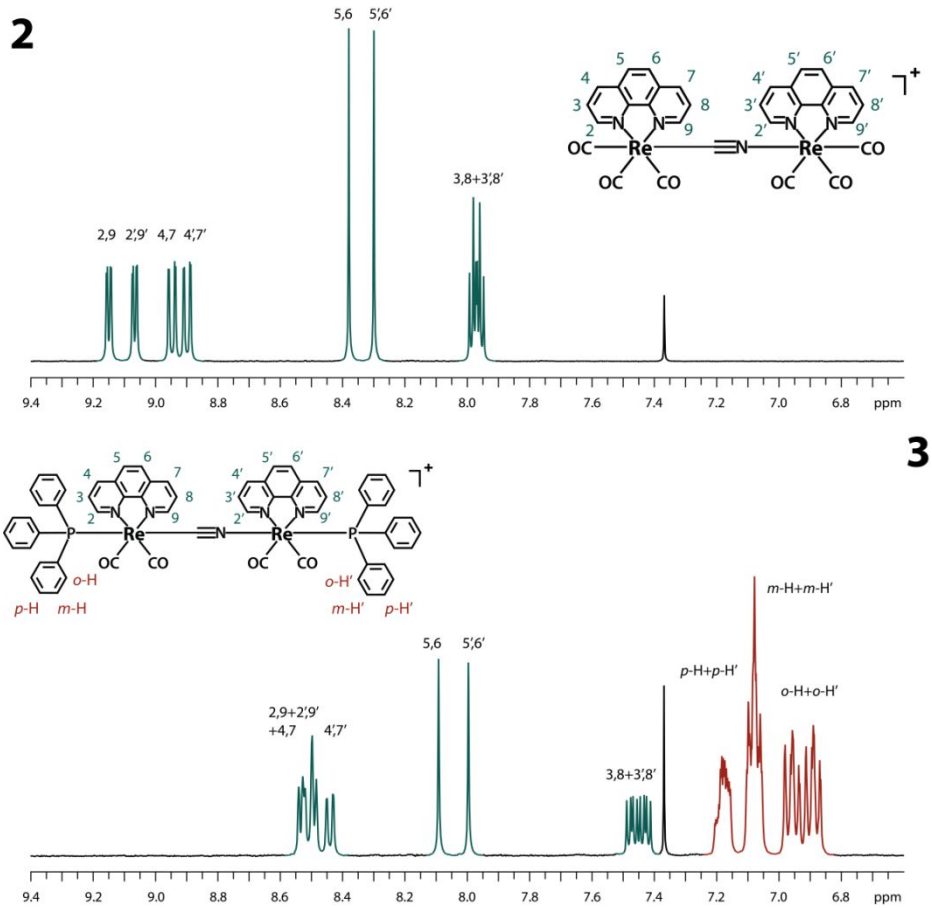

Figure S3. ^{1}H NMR spectra of complexes **2**, **3** (400 MHz, acetone-d_6, 298 K).

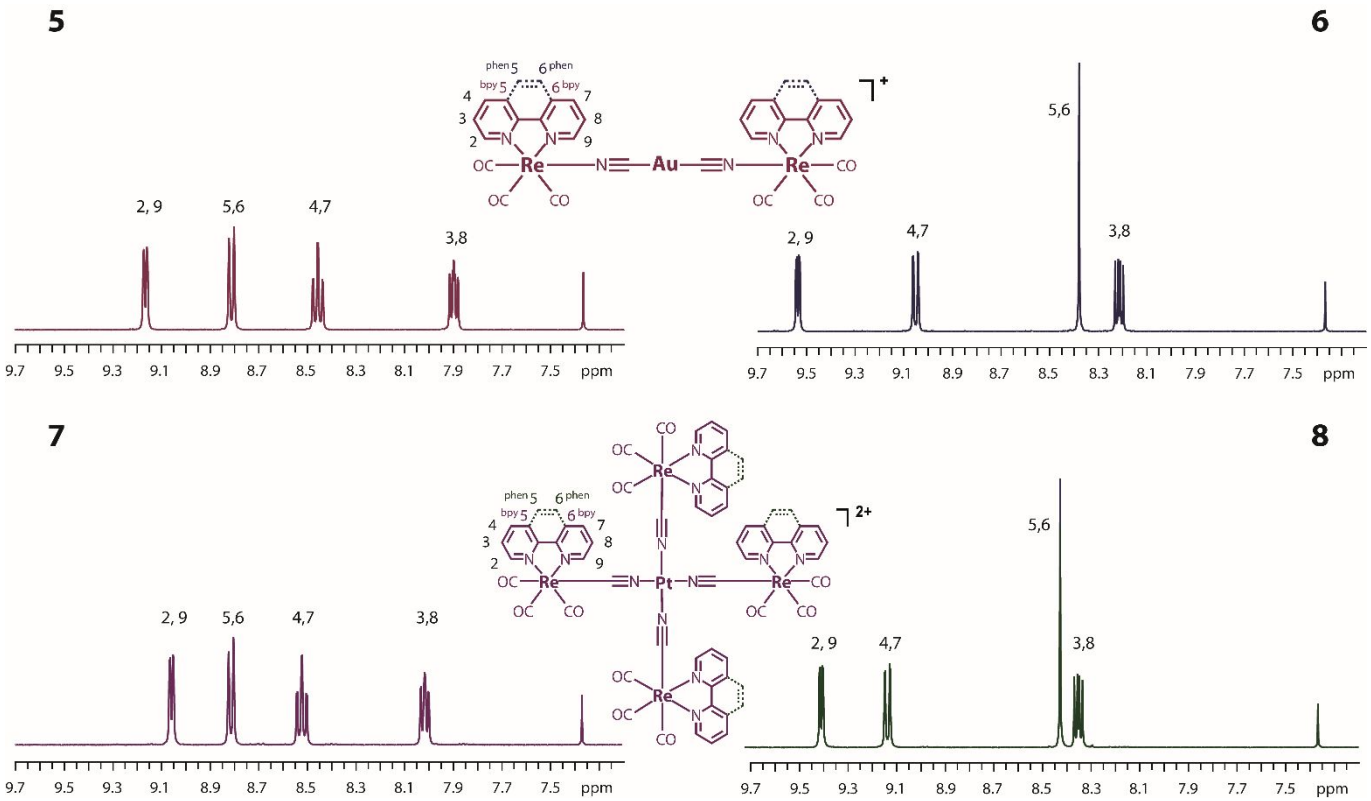

Figure S4. ^{1}H NMR spectra of complexes **5**−**8** in the aromatic region (400 MHz, acetone-d_6, 298 K).

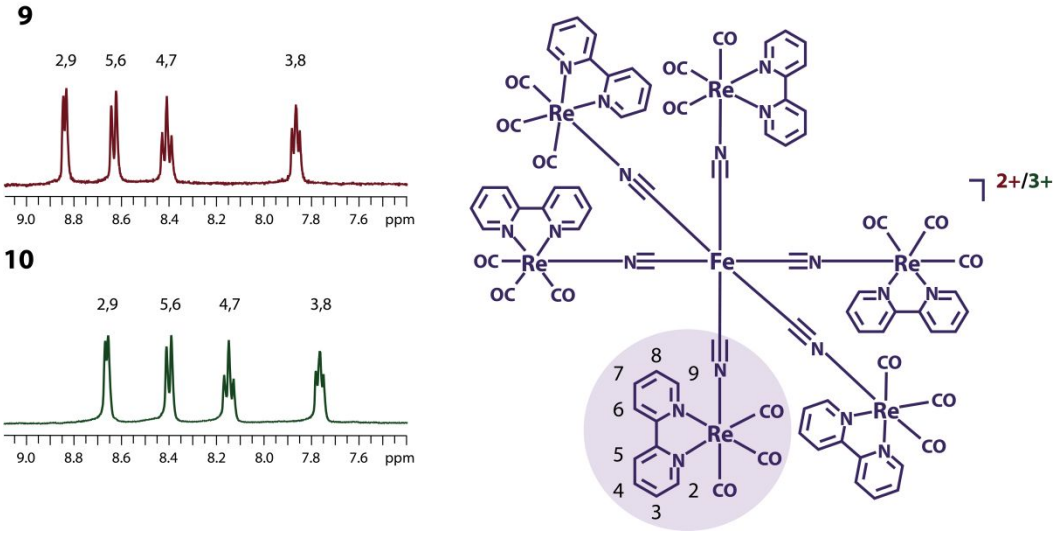

Figure S5. ^{1}H NMR spectra of complexes **9**, **10** (400 MHz, acetone-d_6, 298 K).

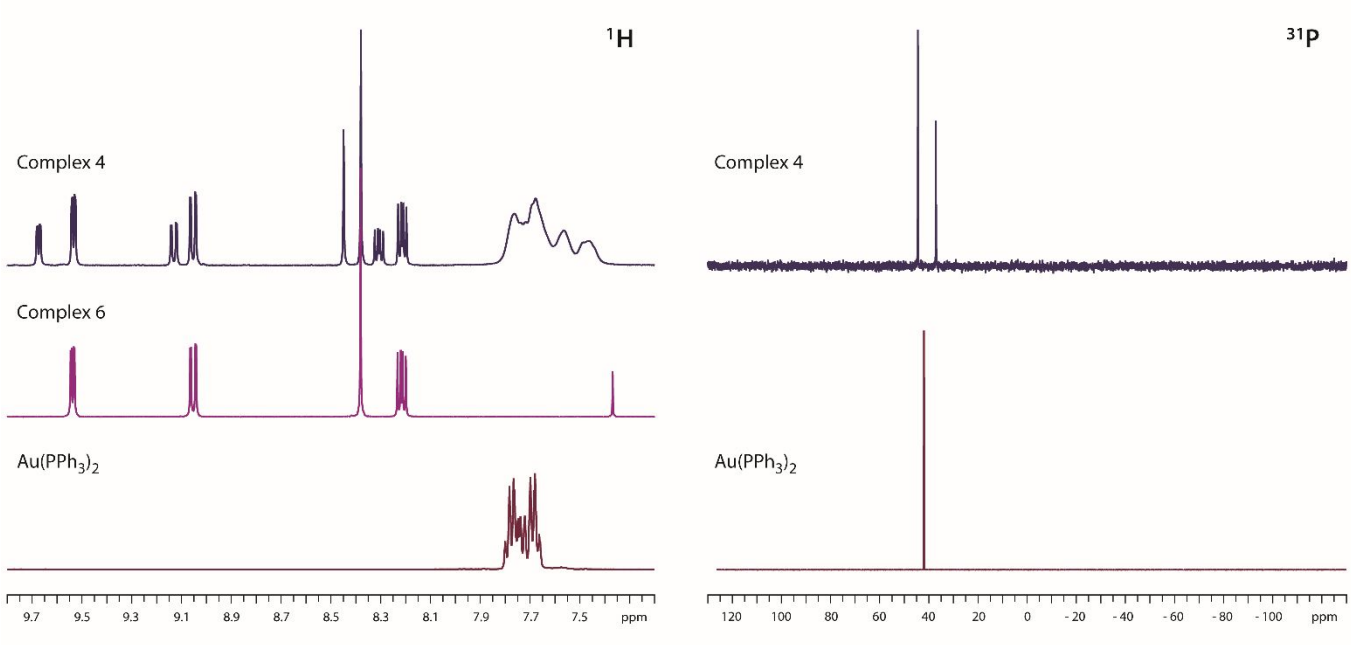

Figure S6. ^{1}H (left) and ^{31}P{^{1}H} (right) NMR spectra of complex **4** (400 and 162 MHz, respectively, acetone-d_6, 298 K) showing that **4** exists as a mixture of three species in solution.

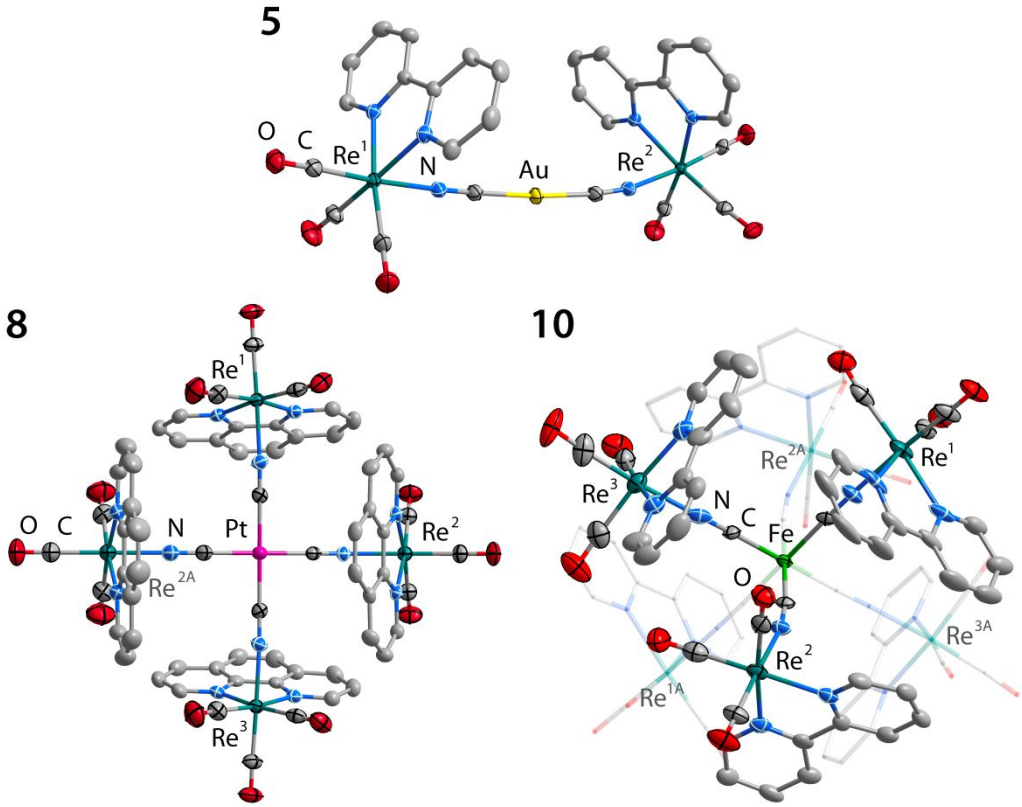

Figure S7. Molecular views of complexes **5**, **8** and **10**. Counterions and hydrogen atoms are omitted for clarity. Thermal ellipsoids are shown at the 50% probability level.

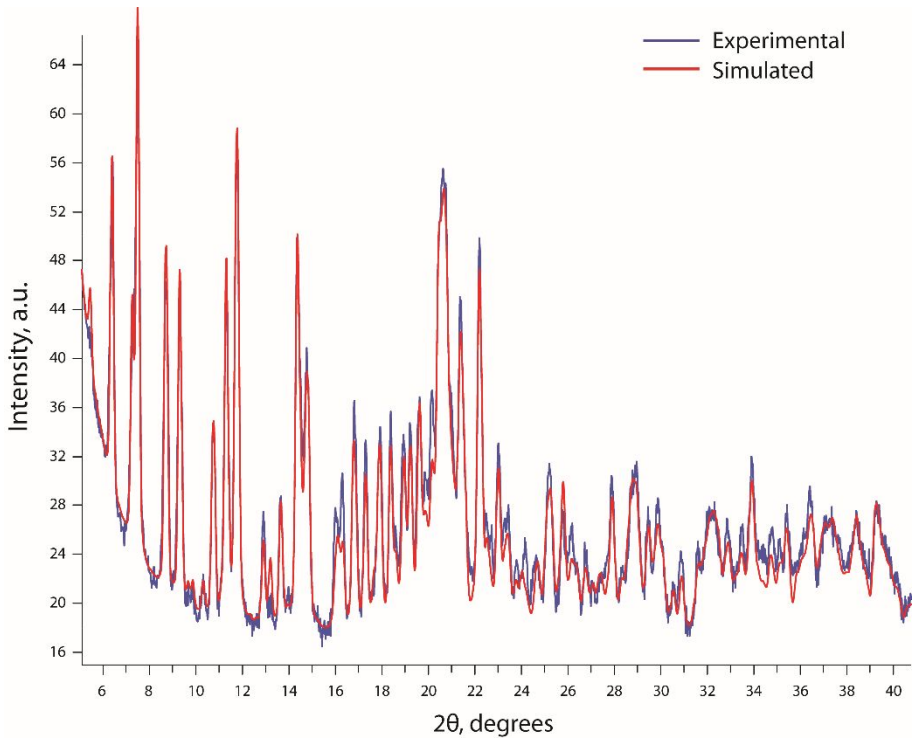

Figure S8. Experimental and simulated (from single crystal data) powder X-ray diffraction patterns for complex **4**.

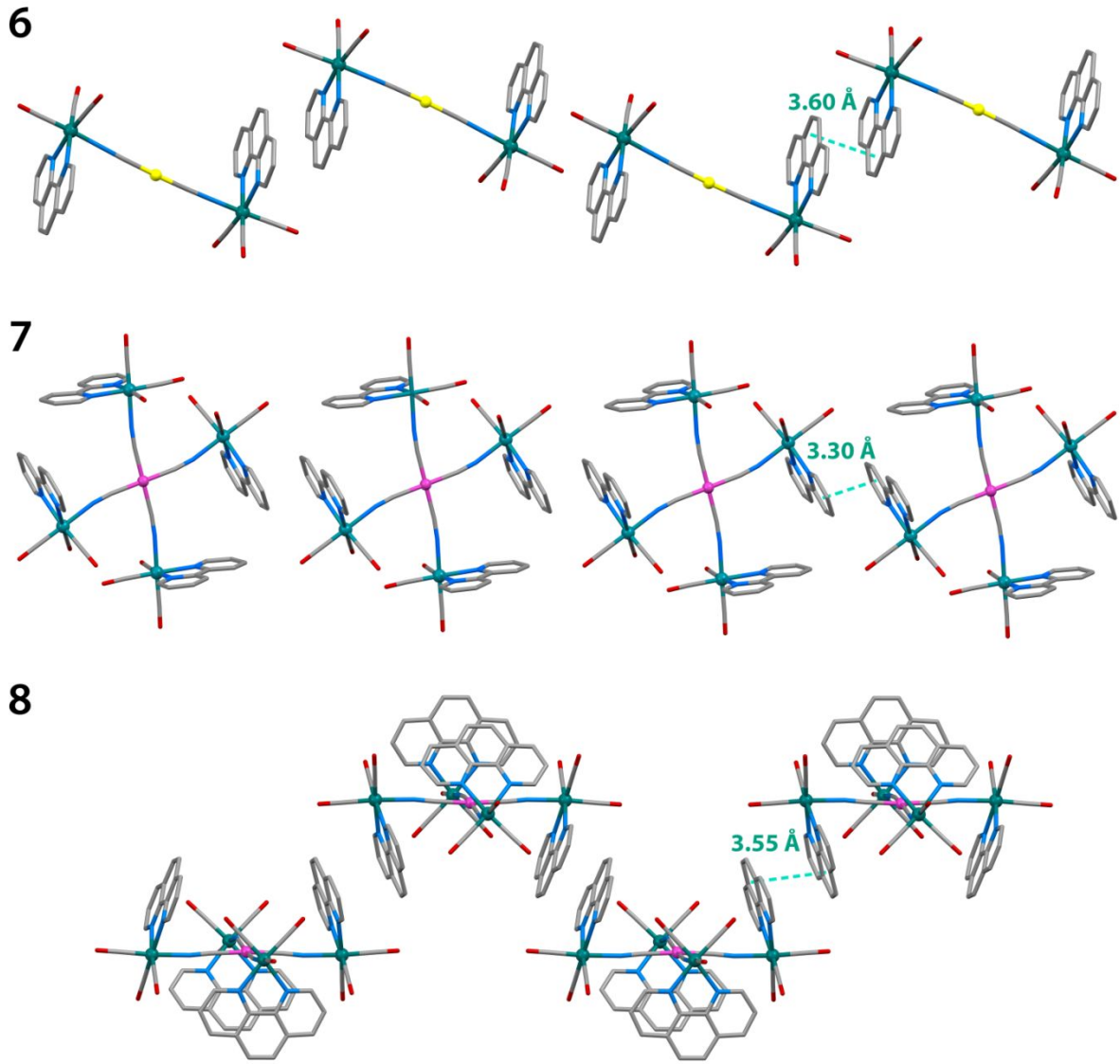

Figure S9. Molecular views of **6−8** showing intermolecular stacking interactions.

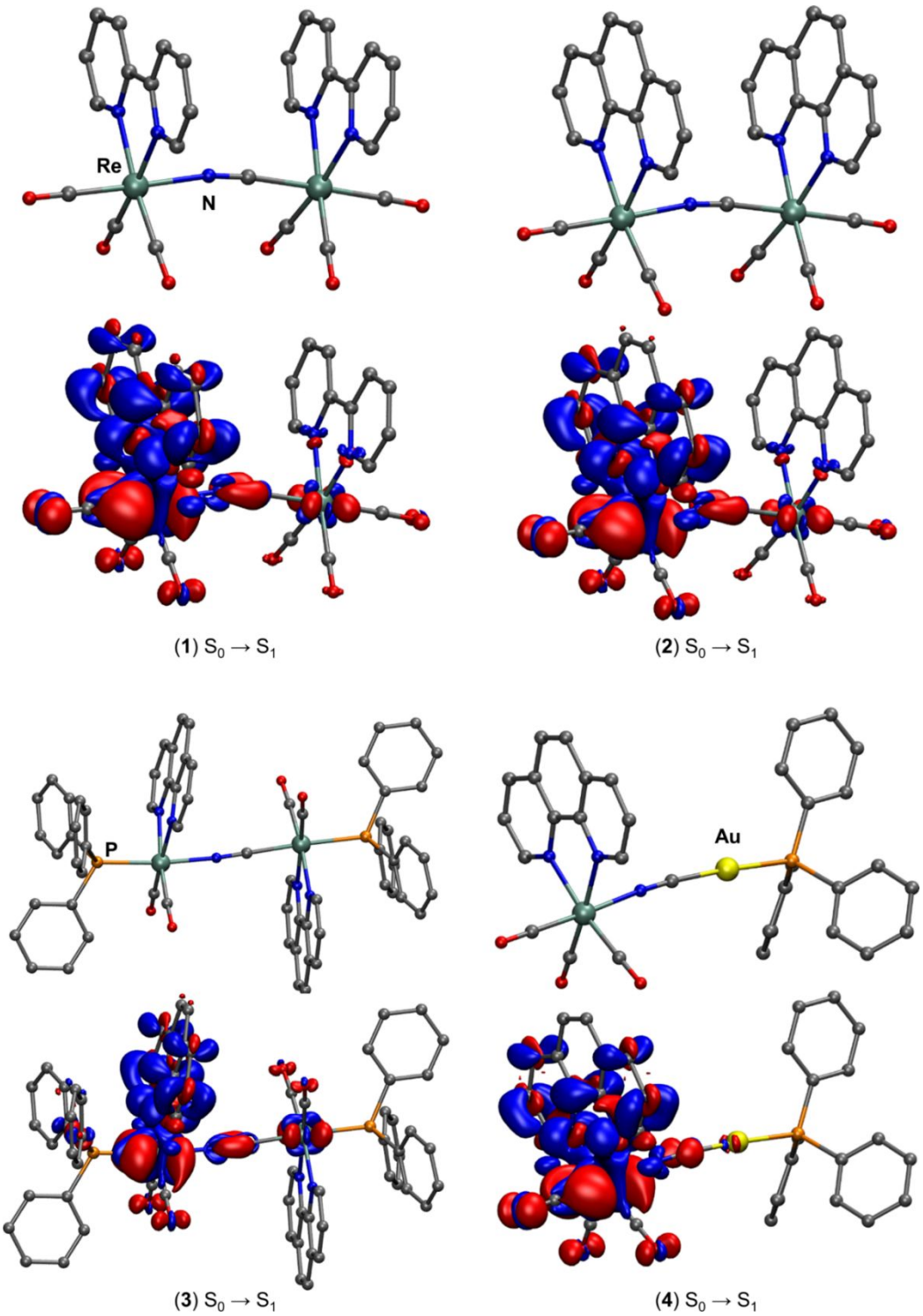

Figure S10. Optimized structures and $S_0 \rightarrow S_1$ electron density difference plots of complexes **1–4** (isovalue 0.002 a.u.). In **1**–**3**, the and $T_1 \rightarrow S_0$ emission is essentially opposite to the $S_0 \rightarrow S_1$ excitation (for **4**, the T_1 state could not be converged due to numerical issues). During the electronic transition, the electron density increases in the blue areas and decreases in the red areas. Hydrogen atoms are omitted for clarity.

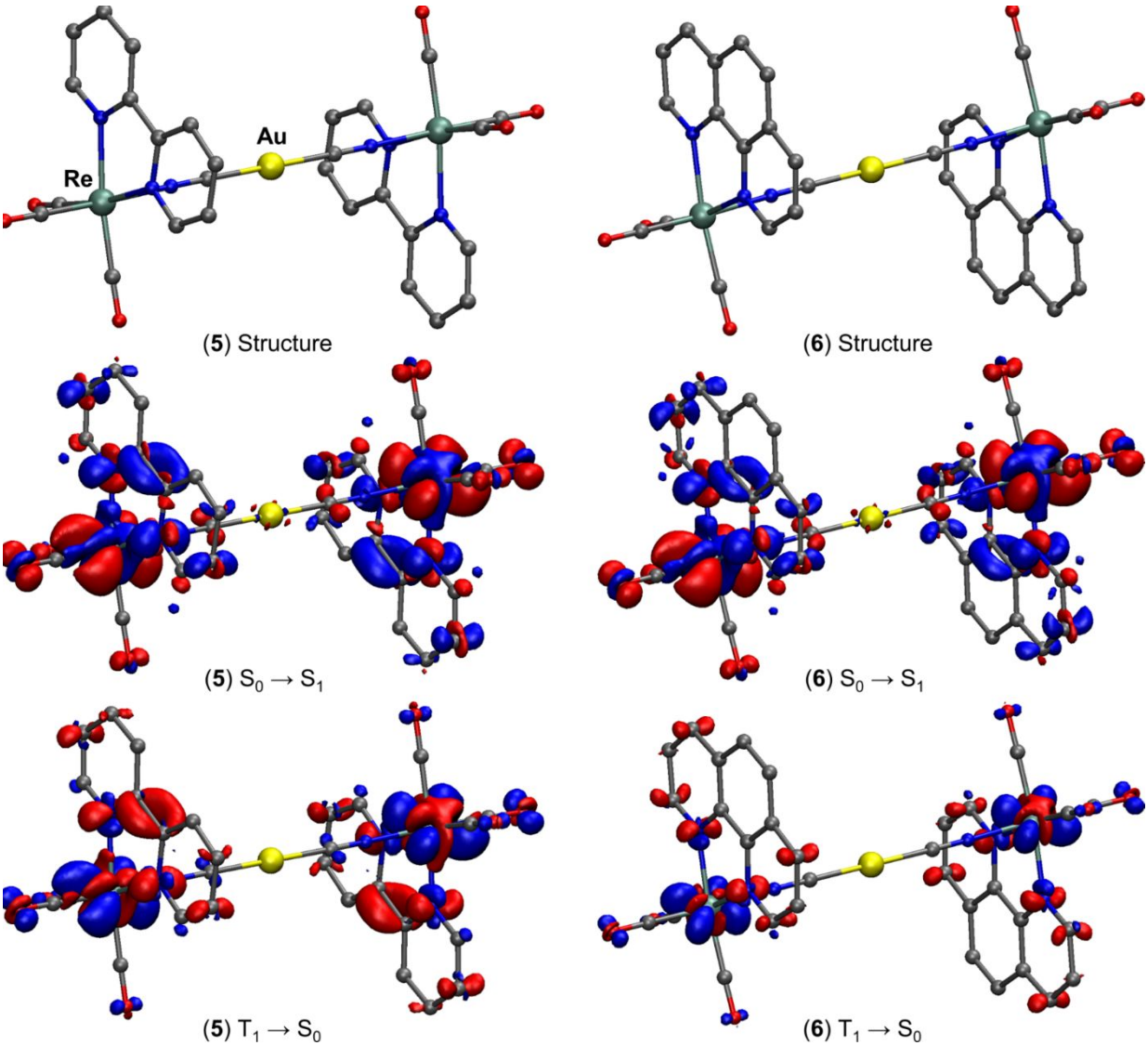

Figure S11. Optimized structures and electron density difference plots for $S_0 \rightarrow S_1$ and $T_1 \rightarrow S_0$ transitions of complexes **5** and **6** (isovalue 0.002 a.u.). During the electronic transition, the electron density increases in the blue areas and decreases in the red areas. Hydrogen atoms are omitted for clarity.

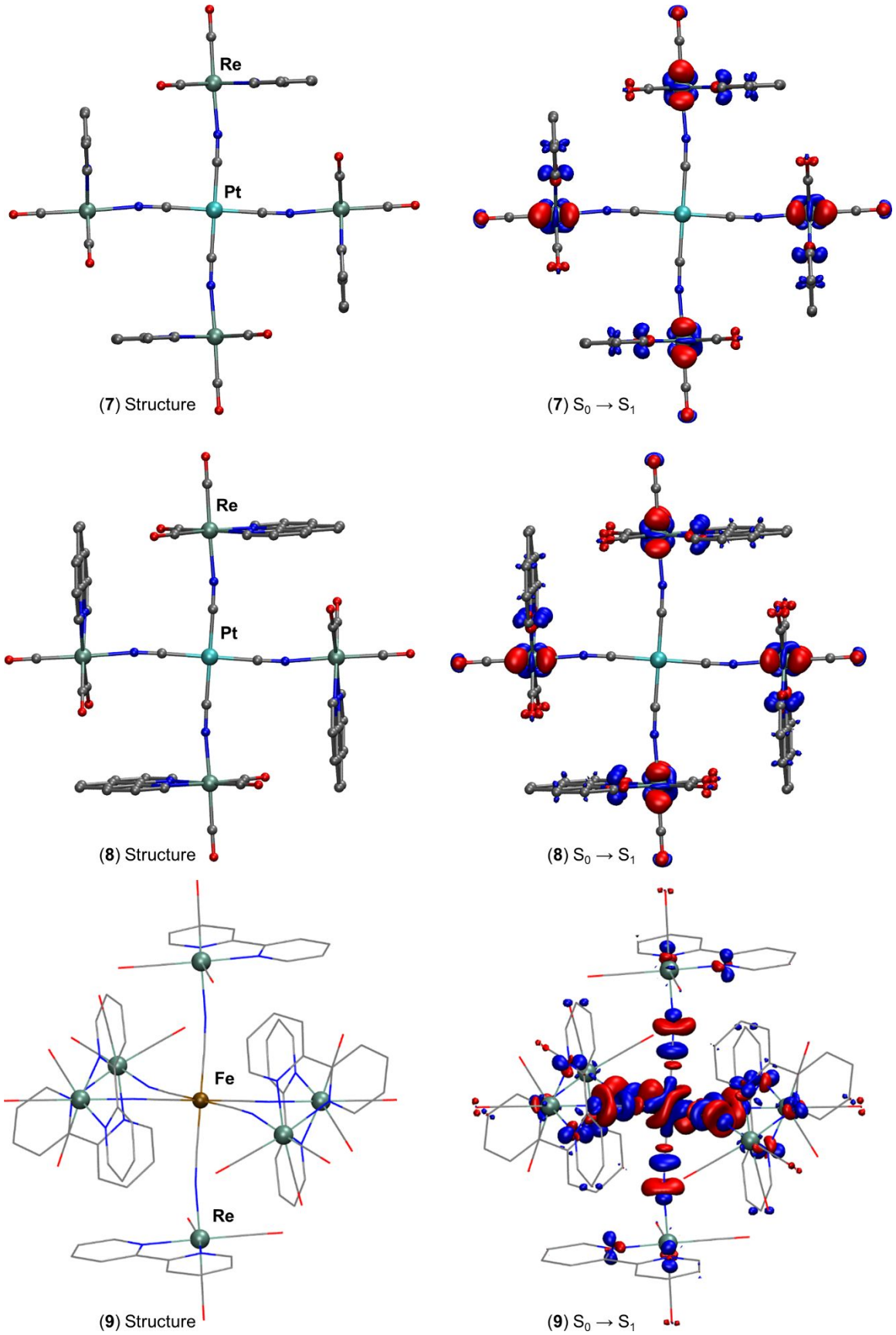

Figure S12. Optimized structures and $S_0 \rightarrow S_1$ electron density difference plots of complexes **7–9** (isovalue 0.002 a.u.). During the electronic transition, the electron density increases in the blue areas and decreases in the red areas. For clarity, non-metallic parts of complex **9** are drawn as line diagrams. Hydrogen atoms are omitted for clarity.

Table S5. HOMO–LUMO gaps and computational photophysical results for complexes **1**–**9** (TD-DFT).

	HOMO–LUMO gap (eV)	λ_{ab} $S_0 \rightarrow S_1$ (nm)	λ_{em} $T_1 \rightarrow S_0$ (nm)[a]
1	3.5	471	693
2	3.5	462	632
3	3.0	559	855
4	3.9	422	
5	3.8	431	538
6	3.8	423	520
7	4.0	397	
8	4.0	391	
9	2.9	547	

[a] In the case of **4** and **7**–**10**, the TD-DFT calculation of the T_1 state could not be converged due to numerical issues.

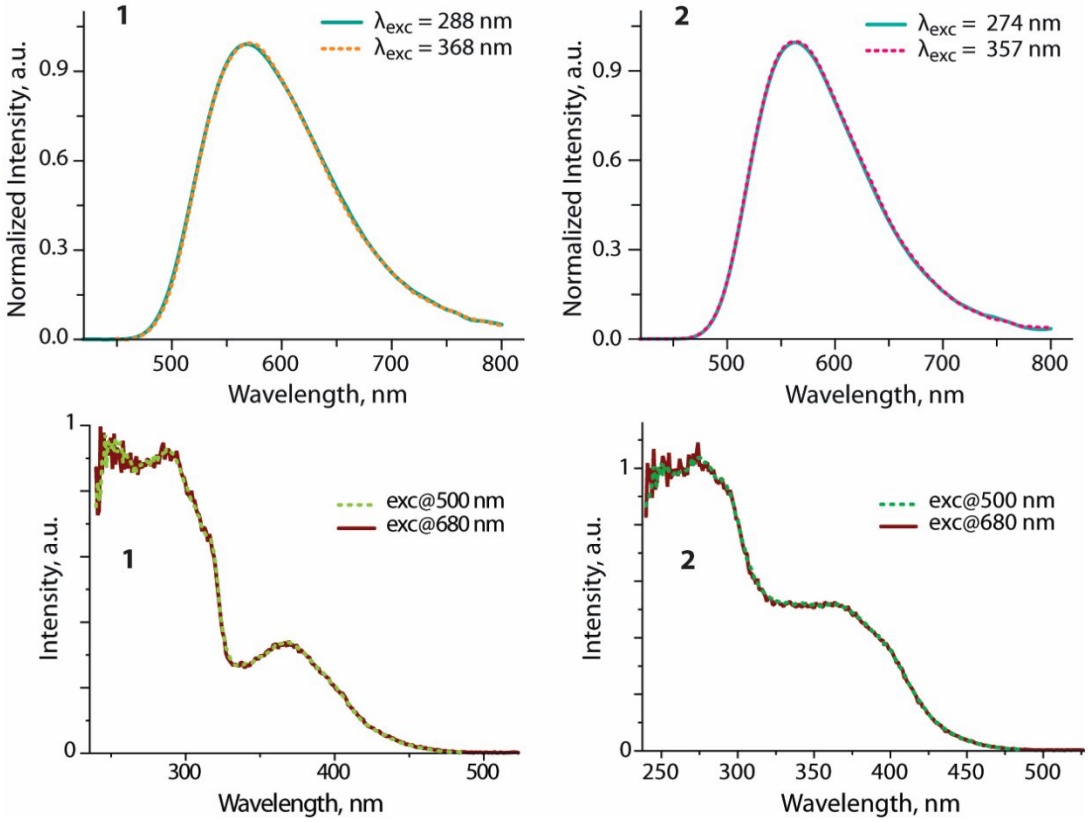

Figure S13. Normalized emission (top) and excitation (bottom) spectra of complexes **1** and **2** in dichloromethane at 298K.

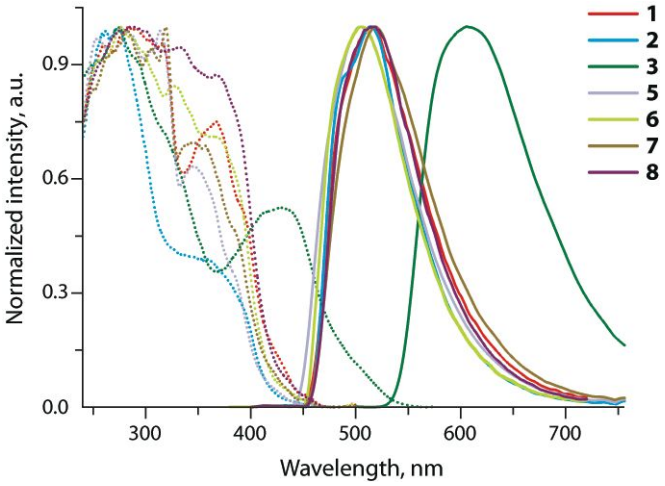

Figure S14. Normalized excitation (dotted lines) and emission (solid lines) spectra of complexes **1**–**3** and **5**–**8** in frozen dichloromethane at 77K.

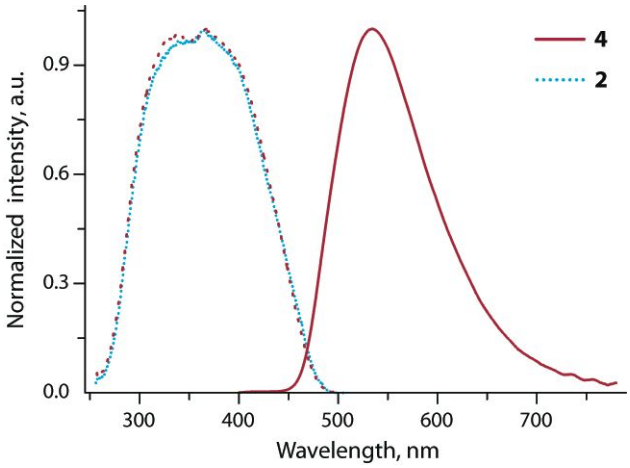

Figure S15. Normalized excitation (dotted line) and emission (solid line) spectra of complex **4** in the solid state at 298K (excitation spectrum of **2** is shown for the comparison).

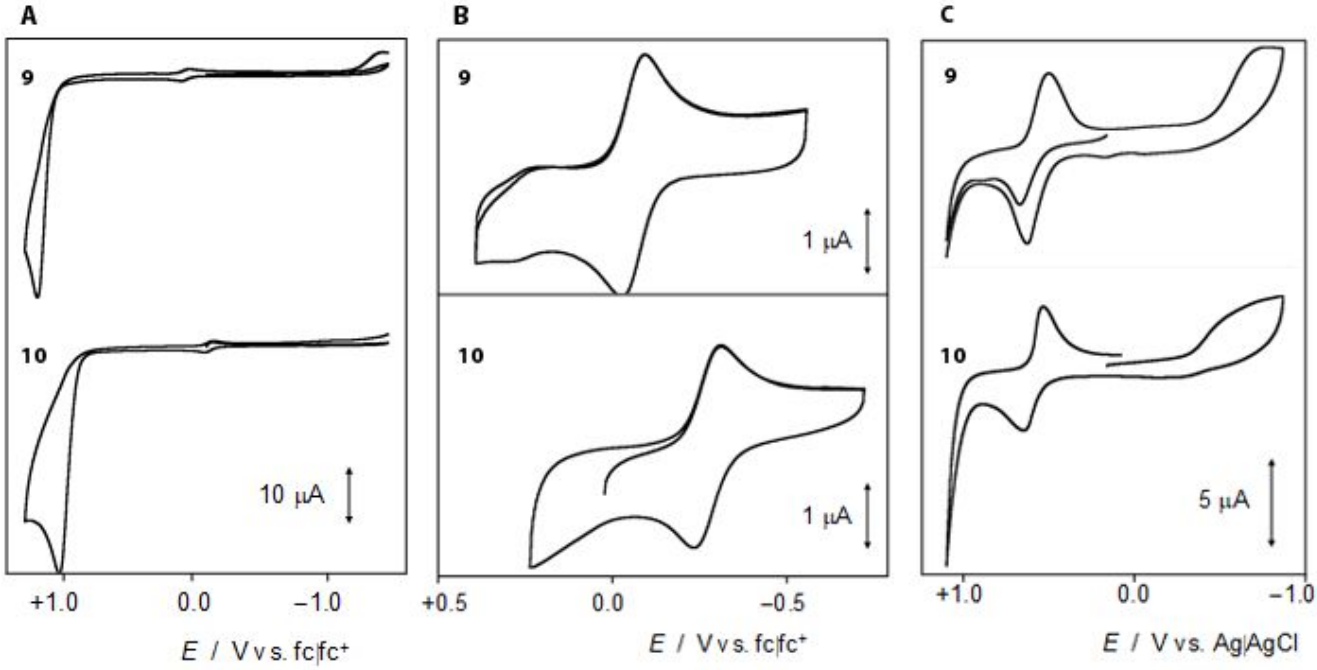

Figure S16. **A**: cyclic voltammograms at glassy carbon electrode for 0.5 mM solutions of complexes **9** and **10** in 0.10 M Bu_4NPF_6/acetone. Potential scan rate 50 mV s^{-1}. **B**: the voltammetric response of the $Fe^{II/III}$ couple. **C**: cyclic voltammograms of microparticulate films of **9** and **10** deposited on glassy carbon electrode in contact with air-saturated 0.50 M NaCl aqueous solution. Potential scan rate 50 mV s^{-1}.

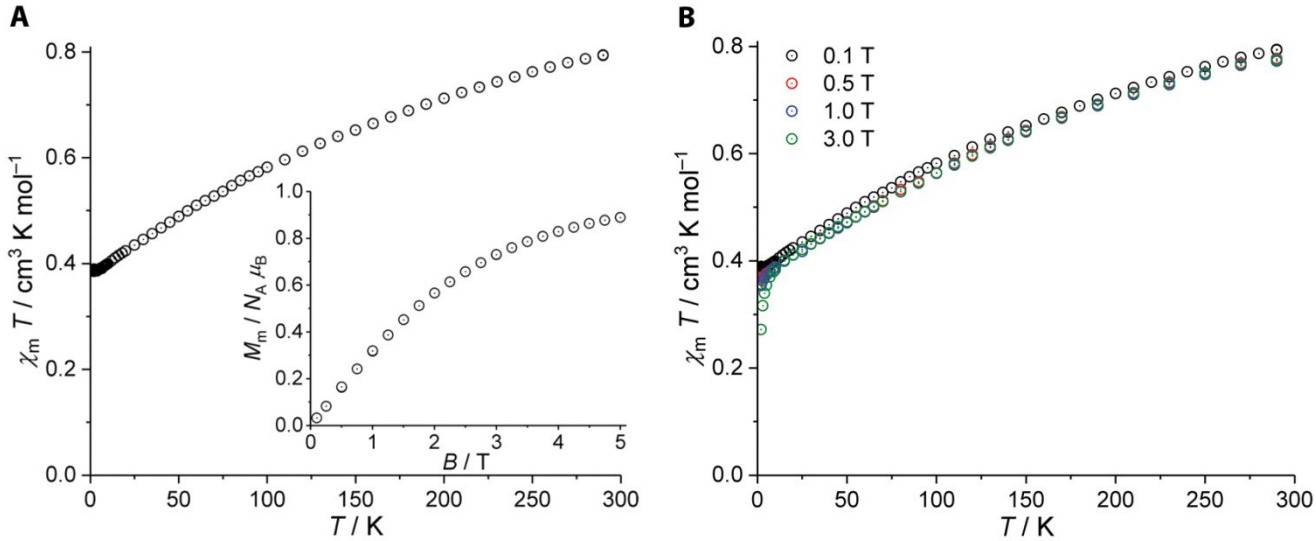

Figure S17. **A**: temperature dependence of $\chi_m T$ of complex **10** at 0.1 T; inset: molar magnetization M_m as a function of the applied field B at 2.0 K. **B**: temperature dependence of $\chi_m T$ of complex **10** at different applied fields B 0.1–3.0 T.